Journal of Molecular Liquids 352 (2022) 118675

Contents lists available at ScienceDirect

Journal of Molecular Liquids

journal homepage: www.elsevier.com/locate/molliq

Molecular modelling aided catalyst design for PAO oils hydrofinishing

Mohammadreza Mehdizadeh [a], Samahe Sadjadi [b,*], Albert Poater [c,*], AmirMohammad Mansouri [d], Naeimeh Bahri-Laleh [a,*]

[a] Polymerization Engineering Department, Iran Polymer and Petrochemical Institute (IPPI), P.O. Box 14965/115, Tehran, Iran
[b] Gas Conversion Department, Faculty of Petrochemicals, Iran Polymer and Petrochemical Institute, PO Box 14975-112, Iran
[c] Institut de Química Computacional i Catàlisi and Departament de Química, Universitat de Girona, c/ Maria Aurèlia Capmany 69, 17003 Girona, Catalonia, Spain
[d] Kermanshah Polymer Petrochemical Company, Kermanshah, Iran

ARTICLE INFO

Article history:
Received 11 January 2022
Revised 29 January 2022
Accepted 31 January 2022
Available online 5 February 2022

Keywords:
Polyalphaolefins
Catalyst
Pd nanoparticles
Hydrofinishing
DFT

ABSTRACT

In an attempt to move towards single metal atom catalysis, the functionalization of halloysite with amino-based ligands, where palladium atoms are complexed, is evaluated here as a pathway. The effect of the nature of the aromatic amine is first evaluated by DFT calculations to find the best one. From a series of ten aromatic amine ligands it is discernible which one has the most complexation capacity to the palladium species, analyzing the structural and electronic properties. After this small exercise of predictive catalysis, the catalyst of choice was then synthesized and characterized experimentally, in addition to conducting catalytic studies. Specifically, its efficiency for polyalphaolefin hydrogenation was investigated in different process conditions. Results demonstrate that the synthesized catalyst could promote polyalphaolefin hydrofinishing at optimum catalyst loading, reaction temperature and hydrogen pressure of 5 wt%, 130 °C and 7 bar, respectively to furnish the final product with bromine index of 55 Br/100 in 96 % yield.

1. Introduction

Halloysite (Hal) is a clay of the Kaolin group with the formula of $Al_2(OH)_4Si_2O_5{\cdot}nH_2O$ The most common morphology of this dioctahedral 1:1 clay is tubular [1,2,3]. Actually, halloysite nanotubes (HNTs) drive to the formation of tubular micelles [4,5]. HNTs are unique 1D natural nanofillers with a hollow tubular shape and high aspect ratio [6]. The large hollow lumen of Hal can potentially be used to load functional molecules [7], such as drugs and catalysts. On the other hand, the –OH functionality of Hal surface can be readily applied for the introduction of functional groups and surface modification [8]. Interestingly, the oppositely charged inner and outer Hal surfaces provide an opportunity to tune the surface properties of Hal. These features, as well as high thermal and chemical stability of Hal, and its availability and biocompatibility [9,10], resulted in rapid growth of Hal-based catalysts for various chemical reactions [11,12], including hydrogenation, oxidation, synthesis of organic compounds [13,14,15,16].

Ionic liquids (ILs) are well-known organic salts that have been extensively studied for various scientific fields [17,18,19]. The syntheses of conventional ILs are relatively simple and many organic cations, including aliphatic and aromatic ones can be applied to design new ILs [20,21,22,23,24]. One of the interesting uses of ILs is catalysis. These compounds can not only be used as homogeneous catalysts, but can also be supported and applied for heterogeneous catalysis [25].

Polyalphaolefins, PAOs, are synthetic oils with high oxidation resistance and viscosity index (VI, >125) and low pour points [26]. These oils are extensively employed for high-performance engine lubricants [27,28]. In the field of polymerization [29,30,31], conventionally, PAOs are prepared through oligomerization of monomers, such as 1-decene [32,33]. Notably, the obtained PAOs contain–C = C double bonds in their backbones, resulting in their low stability at elevated temperatures [34]. One solution for improving the properties of PAO for high temperature applications is hydrofinishing. In this process the olefinic bonds of PAO are reduced and consequently, the stability of PAO will increase. Similar to all hydrogenation processes [35], the use of a hydrogen source and a catalyst is imperative for the hydrogenation

* Corresponding authors at: Polymerization Engineering Department, Iran Polymer and Petrochemical Institute (IPPI), P.O. Box 14965/115, Tehran, Iran (Samahe Sadjadi); Institut de Química Computacional i Catàlisi (Albert Poater); Departament de Química, Universitat de Girona, c/ Maria Aurèlia Capmany 69, 17003 Girona, Catalonia, Spain (Naeimeh Bahri-Laleh)

E-mail addresses: s.sadjadi@ippi.ac.ir (S. Sadjadi), albert.poater@udg.edu (A. Poater), n.bahri@ippi.ac.ir (N. Bahri-Laleh).

https://doi.org/10.1016/j.molliq.2022.118675
0167-7322/

of PAO. Unfortunately, this process frequently requires harsh reaction conditions that make it high risk and costly.

Continuing our efforts to develop hydrogenation catalysts [1,36], we recently focused on the combined experimental and computational studies to shed light into the effective parameters on the design and synthesis of the catalysts [38,54,48]. In this project, we intend to report a novel heterogeneous catalyst for the hydrogenation of PAO under mild reaction conditions. The palladium is complexed on amine based ligands supported on halloysite [37]. To synthesize the catalyst, Pd/Hal-Py, Hal was surface modified by multi-nitrogen and IL containing functional group by successive reactions with (3-chloropropyl)triethoxysilane (CPTES), imidazole, 1,2-dichloroethane and an aromatic amine. To appraise the effect of the nature of the aromatic amine and find the best one, ten aromatic amines included in Fig. 1 have been selected and their performance was studied by the computational study. The catalyst of the choice was then synthesized, characterized and investigated for PAO hydrogenation.

2. Experimental

2.1. Materials

In this project, PAO has been prepared and then hydrogenated by a new heterogeneous catalyst. 1-decene, $AlCl_3$ and NaOH were used (provided from Merck Co. Germany) to synthesize PAO. Catalyst synthesis was conducted using the following chemicals and solvents: Hal, CPTES, potassium carbonate (K_2CO_3), imidazole, 1,2-dichloroethane, acetonitrile, 2-aminopyrimidine, toluene, $NaBH_4$ and methanol (MeOH), all purchased from Sigma-Aldrich and used without further purification.

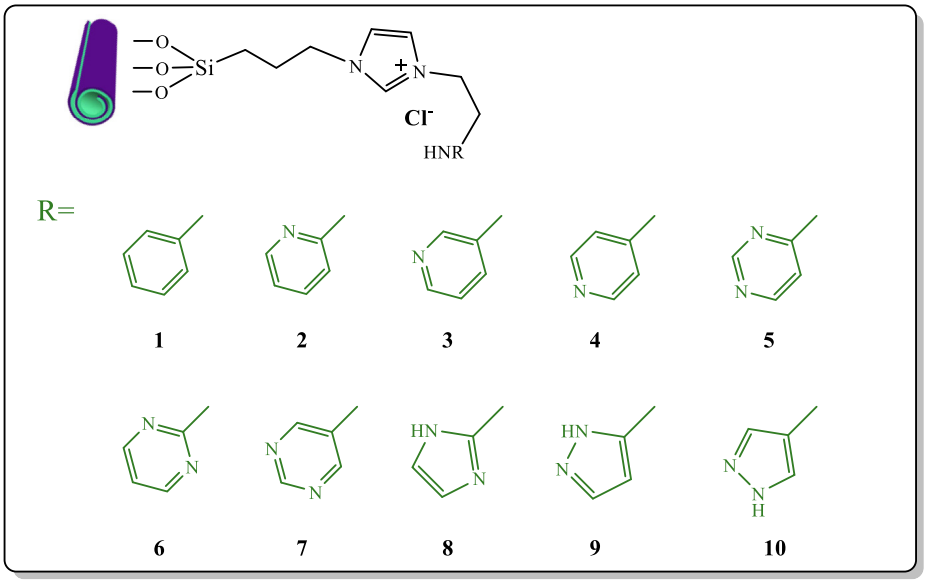

Fig. 1. a) The structure of ligands surveyed in molecular modelling studies and b) schematic synthetic route of the final hydrogenation catalyst.

2.2. Apparatus and equipment

To verify the formation of Pd/Hal-Py, the following analyses were conducted: transmission electron microscopy (TEM, Philips CM30300Kv instrument), thermogravimetric analysis (TGA, METTLER TOLEDO apparatus, heating rate of 10 °C min^{-1}, under O_2 atmosphere), X-ray diffraction (XRD, Siemens, D5000 apparatus), Fourier transform infrared (FTIR, BRUKER, EQUINOX 55 using KBr pellet), inductively coupled plasma (ICP, Vista-pro apparatus), Brunauer–Emmett–Teller (BET, Belsorp Mini II device, with preheating of the samples for 3 h at 150 °C), energy dispersive spectroscopy (EDS, TESCAN instrument), and elemental mapping analysis.

Gel permeation chromatography of the synthesized PAO was performed using GPC Agilent 1100, including PS standards for molecular weight calibration and THF as solvent. Bromine index of the hydrogenated PAO was measured according to the ASTM D2710 procedure.

The NMR spectrometer used to measure of the hydrogenation yield (by ^{1}H NMR test) and branching type (by ^{13}C NMR test) was Bruker DRX400MHz NMR spectrometer (in deuterated chloroform at 25 °C).

2.3. Preparation of the catalyst

Synthesis of the catalyst consists of five consecutive steps, the detail of each is as follows:

2.3.1. Synthesis of Hal-Cl

In the first step of the synthesis of the catalyst, pristine Hal was reacted with CPTES. To this purpose, Hal (3 g) was suspended in dry toluene (60 mL) and sonicated for 20 min. CPTES (2.5 mL) was then added to the aforesaid suspension and the mixture was refluxed for 24 h under Ar atmosphere at 110 °C. At the end of the reaction, the reaction vessel was cooled to 25 °C and the solid was separated via centrifugation. The obtained solid (Hal-Cl) was used for the next step after washing with toluene (2 × 5 mL) and dying at 80 °C overnight.

2.3.1.1. Synthesis of Hal-Im. In the next step, the as-prepared Hal-Cl (2.7 g) and potassium carbonate (1.36 g) were mixed in acetonitrile (50 mL). Subsequently, a solution of Im (0.01 mol) in acetonitrile (15 mL) was added and the resulting mixture was refluxed overnight. Upon completion of the reaction, the precipitate was collected via centrifugation, washed repeatedly with deionized water and dried at 80 °C overnight.

2.3.1.2. Synthesis of Hal-DCl. A mixture of Hal-Im (2.3 g) and 1,2-dichloroethane (2.15 mL) in acetonitrile (50 mL) was refluxed overnight. At the end of the reaction, the obtained precipitate was separated and washed with acetonitrile several times, and dried at 50 °C in a vacuum oven.

2.3.1.3. Synthesis of Hal-Py. The as-prepared Hal-DCl (2 g) was suspended in dry toluene (50 mL) and then 2-amino pyrimidine (0.01 mol) was added and the resulting mixture was refluxed at 110 °C for 24 h under argon atmosphere. At the end, the solid was collected, washed with toluene, and dried in oven at 80 °C overnight.

2.3.1.4. Synthesis of Pd/Hal-Py. In the last step of the synthesis of the catalyst, palladium nanoparticles were stabilized on Hal-Py via wet-impregnation method. Briefly, a solution of $Pd(OAc)_2$ (0.051 g) in acetonitrile (5 mL) was slowly introduced to the stirring mixture of Hal-Py (1.7 g) in acetonitrile (20 mL). The mixture was stirred at room temperature under argon atmosphere for 1 h. Afterwards, a fresh solution of $NaBH_4$ in MeOH was prepared and gradually (within 15 min) added to the aforesaid suspension. Stirring was continued under argon atmosphere for 1 h. Upon completion of the reaction, the black solid was separated via centrifugation and dried at 40 °C overnight, Fig. 1b. The Pd content of Pd/Hal-Py was measured to be 2 wt%.

2.4. PAO synthesis

PAO has been synthesized by using the procedure developed in our laboratory [38]. Briefly, the reaction vessel was first prepared by purging Ar gas at 80 °C for 1 h. Subsequently, the oligomerization catalyst, $AlCl_3$ (5 g), was placed in the reactor and the mixture of 1-decene monomer (500 g) with 0.3 mL deionized water (as electron donor) was introduced. The ratio of $H_2O/AlCl_3$ was 1:2. After stirring the reaction mixture for 50 min at 100 °C, the as-prepared PAO was separated and rinsed with sodium hydroxide solution (5 wt%) several times. The obtained viscose oil was then heated under −0.8 bar vacuum up to 250 °C to furnish the pure PAO. The yield of the oligomerization process was 86 %.

2.5. Hydrogenation of PAO

Hydrogenation of PAO was accomplished in a stainless steel reactor. First, the humidity of the reactor was removed by purging dry nitrogen at 100 °C for 1 h. In the next step, Pd/Hal-Py (0.4 g) and PAO (8 g) were placed into the reactor, H_2 gas with pressure of 7 bar was applied and the reactor was heated to 130 °C. Using a magnetic stirrer, the reaction mixture was vigorously agitated (700 rpm) for 8 h. At the end of the reaction, the reactor was cooled and the catalyst was separated. To recover and reuse the catalyst, it was rinsed with hexane three times and dried at 80 °C overnight. The yield of the hydrogenated PAO was measured using ^{1}H NMR.

2.6. Computational details

Gaussian 16 package was applied for conducting molecular modelling simulations [39]. The geometry optimizations were performed using B3LYP, *i.e.* the hybrid GGA functional of Becke-Lee, Parr, and Yang [40,41,42]. In the case of non-metal atoms (*i.e.* C, H, N, O, Al, Si and Cl) the split-valence basis set (Def2SVP keyword in Gaussian) [43,44] was used, whereas for Pd the small-core quasi-relativistic Stuttgart/Dresden effective core potential, with an associated valence basis set (standard SDD keywords in Gaussian16) was adopted [45,46,47].

The geometry optimizations were carried out without symmetry constraints, including the Hal fragment because of its flexibility [48], and the characterization of the stationary points was performed by analytical frequency calculations.

To approve the nature of the stationary points, frequency calculations were carried out. The effect of the solvent on the wet-impregnation process for the stabilization of Pd nanoparticles on the support was surveyed according to the polarizable solvation model (SMD), variation of IEFPCM of Truhlar and co-workers [49], applying toluene, acetonitrile, methanol, using the B3LYP functional and the Def2TZVP basis set, including explicit dispersion corrections to the energy through the Grimme D3 method [50]. For the sake of consistency, the latter calculations were also performed without including the SMD model. The reported free energies in this work include energies obtained at the B3LYP-D3/Def2TZVP ∼ sdd//B3LYP-D3/Def2SVP level of theory corrected, with zero-point energies, thermal corrections and entropy effects evaluated at 25 °C with the BP86/Def2SVP ∼ sdd method in the gas phase, omitting corrections of entropy and standard state of 1 M concentration in solution [51].

Steric maps and free volume, $\%V_{Free}$, of the designed catalysts were obtained using the SambVca2 package of Cavallo and coworkers [52,53].

3. Results and discussion

3.1. Simulation results

To fulfill the requirements of an efficient catalyst in PAO hydrogenation process, suitable inorganic carriers should possess appropriate sites for the absorption of active metal (here Pd), in order to minimize its leaching during the experiment. In this regard, organic ligands undoubtedly play an important role in Pd grabbing. To get a competent wrapper around the active metal, the 10 new ligands in Fig. 1 were designed that benefit from N atoms and an ionic liquid (IL) moiety, first in silico tested. All of these structures play a prominent role in nitrogen atoms together along with IL to minimize catalytic leaching in heterogeneous catalysis [1,48,54]. They actually differ in the structure of the anchor fragment as i) the size of the aromatic ring (5- or 6-member), ii) the number of N atoms in the aromatic ring and iii) the position of N relative to the anchor point.

To decrease the immensity and cost of laboratory experiments, all ligand candidates designed for Pd binding, which is frequently used in hydrogenation catalysis, were analyzed computationally. According to the energy results in Table 1, we could not find a clear correlation between the ring size and the number of N atoms of the anchoring ring structure with G_{Bind} (corresponding to the binding energy of the palladium center on the model of halloysite with the amine ligand). In fact, the designed ligands almost rendered large binding energies (>20 kcal/mol) with the maximum efficiency of ligand **6** revealing G_{Bind} of 32.9 kcal/mol. Notably, a similar trend was also observed in the G_{Bind} values including solvent effects, in which ligand **6** exhibited again the highest efficiency. The closest ligands, in terms of absorption energy, were **1**, **4** and **9**, with G_{bind} of −30.8, −31.9 and −30.6 kcal/mol, respectively. However, the next favored ligands, in terms of binding energy, were all the other systems, with an energy difference of about only 2–3 kcal/mol, except for systems **7** and **10**, placed 6.8 and 6.0 kcal/mol above in energy, respectively. Thus, the ten systems range in narrow window of 6.8 kcal/mol. In the next step, the adsorption of Pd(0) on the designed ligands was surveyed in different solvents as reaction media. The solvents chosen were among the most popular ones, *i.e.* acetonitrile, ethanol and toluene. G_{Bind} energies in acetonitrile were larger than in toluene and in ethanol.

Structurally, Fig. 2 includes the structural shapes of systems **6**–**8** bearing the interaction of Pd on the amine-based ligands (see Figure S1 for the complete series of systems **1**–**10**). The interaction of the palladium with imidazole takes place in all cases through the backbone, *i.e.* the unsaturated C = C bond. And on the other hand, there is a Pd-C or Pd-N interaction, even multiple and/or combined, but in cases where the binding energy is greater it is through a simple Pd- N link. In fact, for the best system, **6,** the distance is 2.211 Å and it might seem worse than system **8** where it even decreases to only 2.155 Å. But this is compensated in the system **6** by a lower tension of the angles. Thus, the Pd-N link of system **8** presents as the worst angle with a Pd-C link of 115.1°, angle clearly lower than 122.5° by **6**. Analyzing the $\%V_{Bur}$ of Cavallo et al. in Table 1 [52,53], it has been verified that they cannot be correlated with the binding energies of the palladium. This contrasts with previously used ligands [55,56], but the reason must be found in the similarity between systems **1**–**10**, with great differentiation with respect to ligands with one or two nitrogen atoms capable of bonding to the metal [57]. Fig. 3 shows that the corresponding steric maps for systems **6**–**8** do not allow to distinguish clearly between them (see Figure S2 for the complete series of systems **1**–**10**).

Due to the bulky structure of a PAO chain, and the position of the C = C bond somewhere in the middle of the chain, its availability at the Pd is very important in a successful hydrogenation reaction. To account further for this effect, the extended model of Hal was further explored for system **6**. The $\%V_{Bur}$ goes up to 69.7%. Thus, even though the sterical hindrance difference is significant, it is not conclusive [58], and it is in the range of $\%V_{Bur}$ for the systems **1**–**10** without this extended model of the Hal.

From both Pd adsorption energy and free volume point of view, catalyst **6** exhibited the best efficiency. In particular, calculations showed the largest binding energy in acetonitrile solvent. Thus, it was synthesized, with the corresponding Pd impregnation, and employed in PAO hydrofinishing experiments in the laboratory experiments.

3.2. Analysis and characterization of Pd/Hal-Py

TEM images of Pd/Hal-Py were recorded to assess whether Hal retains its tubular morphology and to investigate the dispersion of Pd nanoparticles on Hal-Py [59,60]. As presented in Fig. 4, the tubes of Hal are detectable. As displayed, fine particles of Pd nanoparticles (average particle size of 3.49 ± 0.14 nm) with high dispersion are deposited on Hal-Py.

EDS analysis of Pd/Hal-Py in Fig. 5 confirmed the presence of the expected atoms, C, N, O, Si, Al, Cl and Pd, in the structure of the as-prepared catalyst. In fact, the presence of C, O, N and Cl is indicative of the grafted organic functionality on Hal. Using elemental mapping analysis, the dispersion of the atoms present in the structure of the catalyst has been investigated. As shown, Pd nanoparticles are uniformly dispersed. Moreover, high dispersion of C, N and Cl atoms is representative of uniform functionalization of Hal with the organic moiety.

To approve the conjugation of the functional groups in each step, Hal-Im, Hal-DCl and Pd/Hal-Py were characterized via FTIR spectroscopy and the recorded spectra were compared with that of Hal. According to the literature [61], the absorbance bands of Hal are the bands at 3696 cm^{-1} and 3626 cm^{-1} (inner –OH), 1033 cm^{-1} (Si-O stretching), 797 cm^{-1} (symmetric stretching of

Table 1
Binding energies (in kcal/mol) of Pd adsorption on ligands designed in gas and solvent phases, and the corresponding $\%V_{Bur}$ values.

Cat No	G_{Bind} (gas)	G_{Bind} (toluene)	G_{Bind} (ethanol)	G_{Bind} (acetonitrile)	V_{Bur} (%)
1	−30.8	−28.9	−28.6	−29.5	67.1
2	−29.7	−30.2	−30.1	−29.8	67.4
3	−29.7	−28.6	−28.3	−28.8	66.4
4	−31.9	−26.5	−26.2	−28.7	61.5
5	−29.0	−26.9	−27.0	−28.1	61.9
6	−32.9	−28.3	−28.1	−30.1	61.4
7	−26.1	−26.0	−25.8	−25.9	65.1
8	−27.0	−27.1	−28.3	−29.0	59.4
9	−30.6	−29.7	−29.6	−30.1	64.4
10	−26.9	−26.8	−26.9	−27.3	65.3

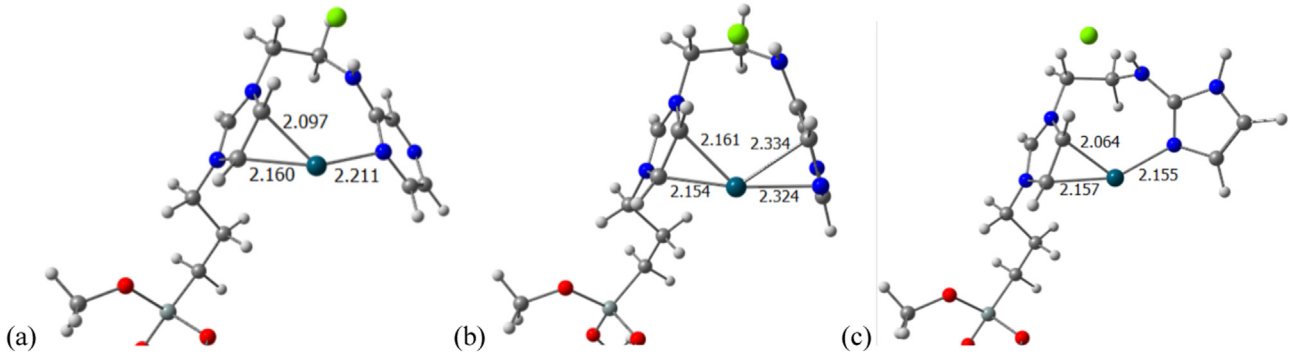

Fig. 2. Systems **6**–**8**, interaction of Pd on the amine-based ligands (selected distances given in Å, Hal has been cut for the sake of clarity).

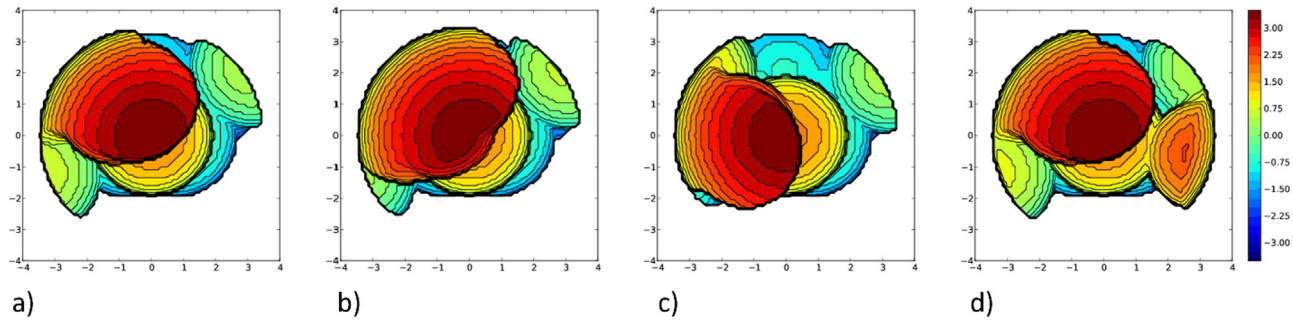

Fig. 3. Steric maps of a-c) catalysts **6**–**8** and d) the extended model of system **6** (xy plane, with the metal placed in the centre and the z axis crossing between both C atoms of the imidazole ring, that are part of the xz plane. Curves are given in Å).

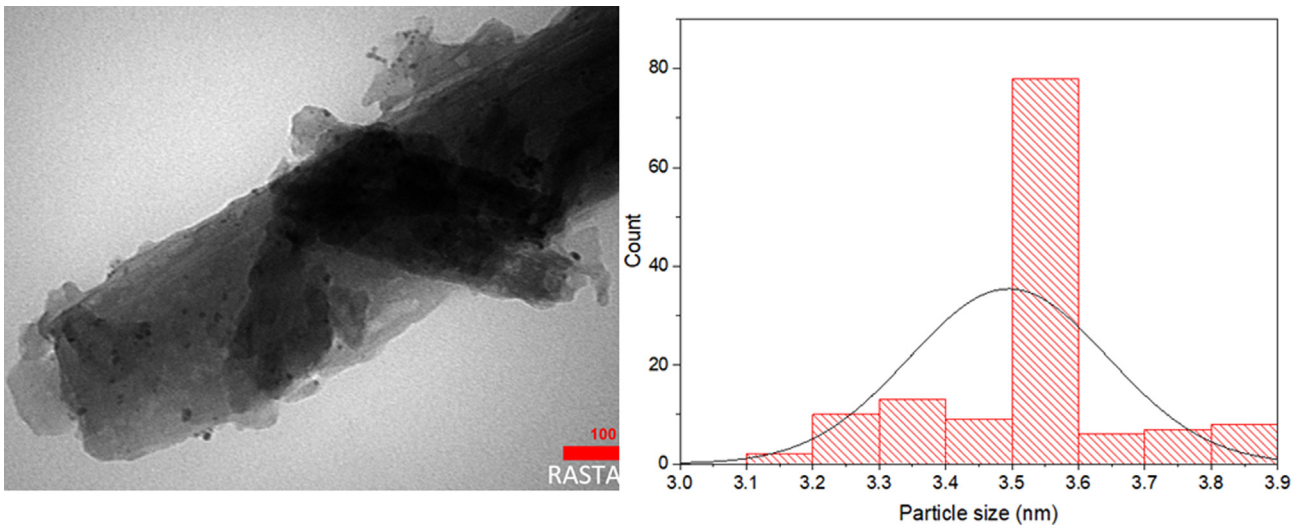

Fig. 4. TEM image (left) and Pd particle size distribution curve of Pd/Hal-Py (right).

Si–O–Si), 691 cm^{-1} (stretching vibration of Al–OH), and 536 cm^{-1} (Al-O-Si vibration). In the FTIR spectrum of Hal-Im, the new bands at 1650 and 2946 cm^{-1} can be ascribed to –C = N and $–CH_2$ functionalities, confirming grafting of Im. FTIR spectrum of Hal-DCl and Pd/Hal-Py are similar to that of Hal-Im. In fact, the characteristic bands of 1,2-dichloroethane and 2-aminopyrimidine overlapped with those of Hal-Im (Fig. 6).

As discussed above, FTIR spectroscopy approved stability of Hal structure upon grafting of the organic functionalities. To further affirm this issue, XRD analysis of Pd/Hal-Py and Hal was carried out. Fig. 7 clearly confirms the similarity of the two XRD patterns. In more detail, the presence of all of the characteristic peaks of Hal (2θ = 12°, 19.9°, 24.7°, 26.6°, 35.0°, 38.3°, 55.0° and 62.4° (JCPDS No. 29–1487) [62,63]) in the XRD pattern of the catalyst without any change in their positions can establish that Hal is structurally stable upon chemical modification. According to the literature, no additional peaks are expected for Pd nanoparticles, as they are very fine and well-dispersed [64].

Specific surface area of Pd/Hal-Py was measured via BET analysis and compared with the value of pristine Hal. It was found that the specific surface area of Hal (48 m^2g^{-1}) significantly decreased upon introduction of the functional group and Pd nanoparticles and reached to 29 m^2g^{-1}.

TG curves of Hal and Pd/Hal-Py are presented in Fig. 8. As depicted, the TG curves of Hal and the as-prepared catalyst are distinguishable. More precisely, in the TG curve of the catalyst three

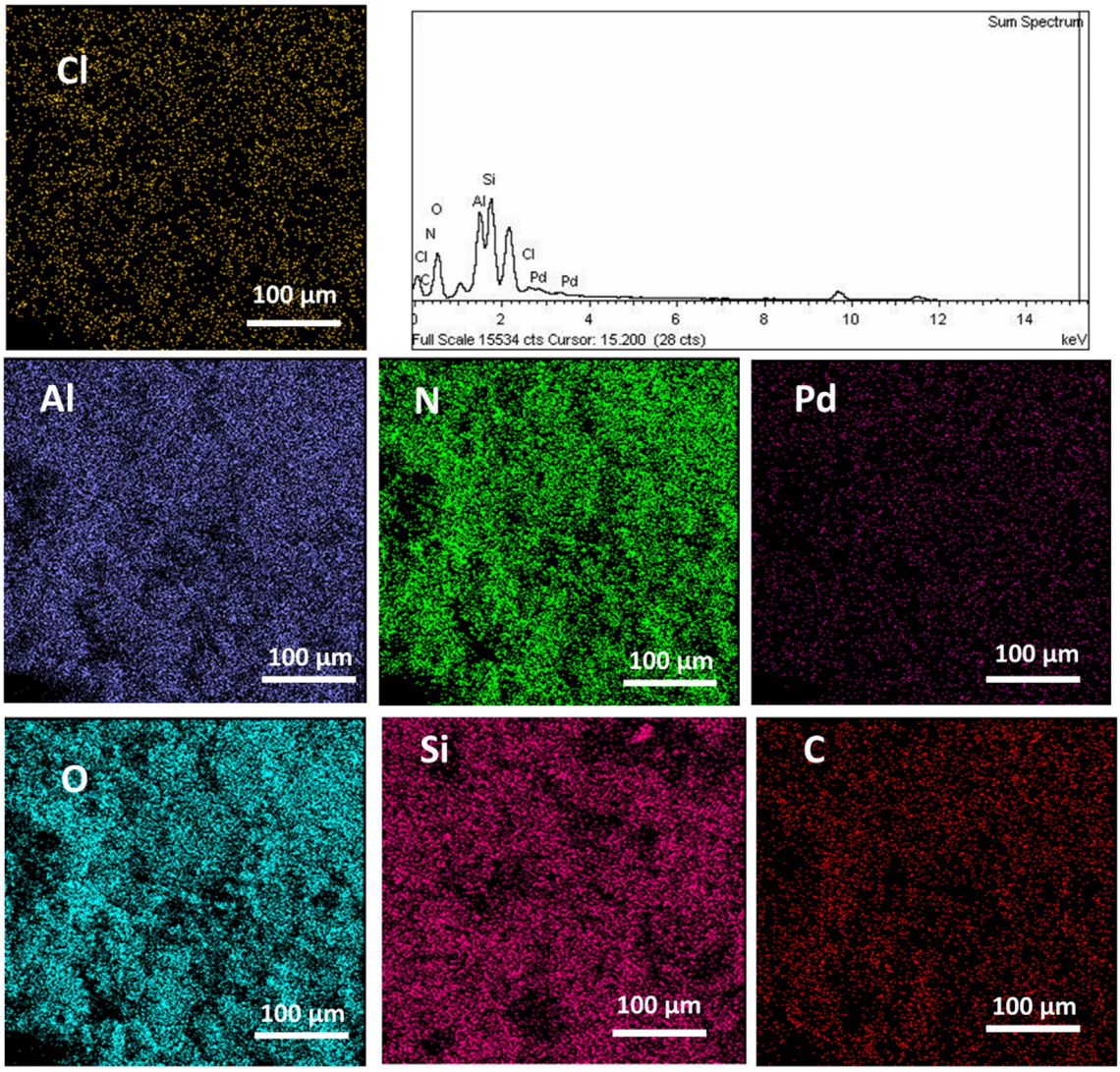

Fig. 5. EDS and elemental mapping analysis of the catalyst.

weight loss steps can be observed, while Hal TG curve showed only two weight loss steps due to the loss of water (~120 °C) and dehydroxylation (at a temperature of 480 °C). In fact, in the TG curve of Pd/Hal-Py, the two weight loss steps of Hal, as well as an additional weight loss at 360 °C that can be assigned to the degradation of the grafted functionality can be detected.

3.3. Activity of Pd/Hal-Py for PAO hydrogenation

Because the use of high hydrogen pressure and reaction temperature can affect the economy and safety of PAO hydrogenation, it was aimed to design a heterogeneous catalyst that could promote this process under mild reaction conditions. In this regard, Pd/Hal-Py, which contains a very low Pd loading, was prepared and characterized. First, the activity of Pd/Hal-Py (5 wt%) for the hydrogenation of PAO at 130 °C and hydrogen pressure of 7 bar was investigated. The result implied that under the aforementioned conditions, hydrogenation yield was 96%. To elucidate the effect of hydrogen pressure, the hydrogenation reaction was repeated under lower hydrogen pressures (6 and 5 bar). It was found that decrease of hydrogen pressure led to the decrease of the yield of PAO hydrogenation. The effect of the reaction temperature was also studied by conducting the hydrogenation reaction at different temperatures (110, 120 and 130 °C) and comparing the results. The results demonstrated that the decrease of the reaction temperature had a detrimental effect on the reaction yield and the highest yield was achieved at 130 °C. Finally, the optimization of Pd/Hal-Py loading was carried out. To this purpose, the yields of PAO hydrogenation in the presence of different loadings of Pd/Hal-Py were measured. It was found that decreasing the catalyst content could also decrease the yield of the reaction. These experiments confirmed that the optimum catalyst loading, reaction temperature and hydrogen pressure were 5 wt%, 130 °C and 7 bar, respectively. Under these conditions, hydrogenated PAO was furnished in 96% with bromine index of 55 Br/100 g. These results established the efficiency of Pd/Hal-Py for promoting PAO hydrogenation under mild reaction conditions.

3.4. Recyclability of Pd/Hal-Py

Motivated by the high catalytic activity of the catalyst under mild reaction conditions, the recyclability of Pd/Hal-Py was also investigated. In fact, recyclability of the catalyst is an important

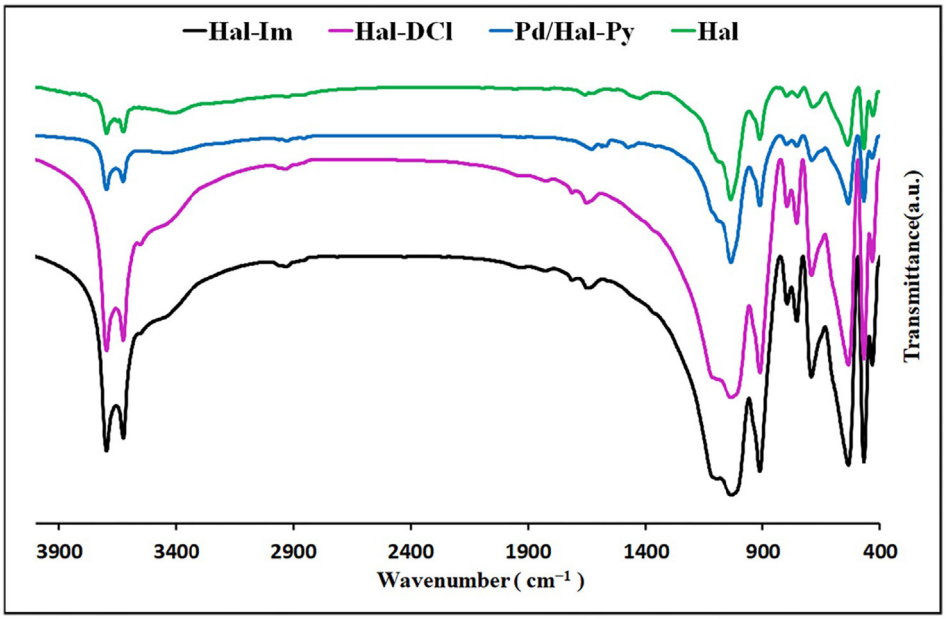

Fig. 6. FTIR spectra of Hal, Hal-Im, Hal-DCl and Pd/Hal-Py.

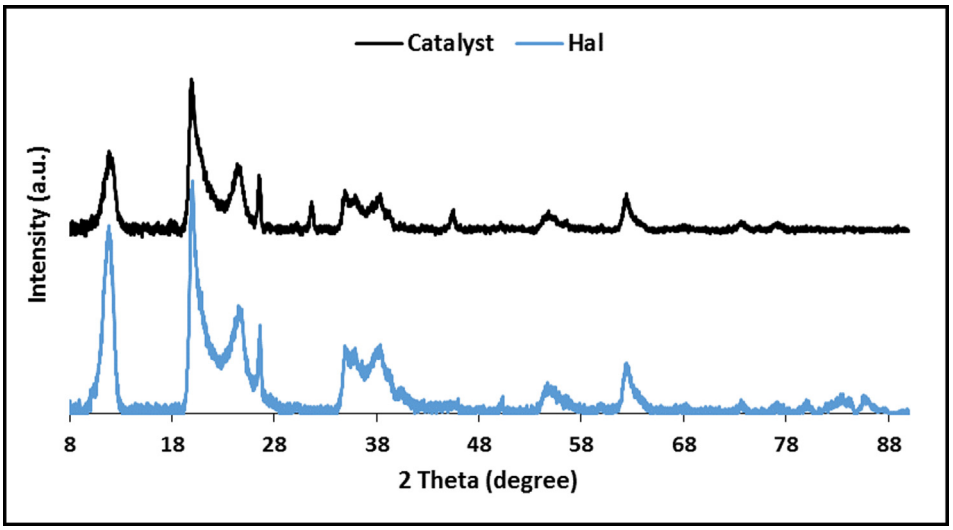

Fig. 7. XRD patterns of Pd/Hal-Py and Hal.

feature of the catalyst that can affect its usefulness. In this regard, the recovered Pd/Hal-Py after the first run of hydrogenation of PAO was used for the second run of the reaction and the yield of the reaction was measured. This cycle, recovery and re-use, was repeated for four runs. For the sake of comparison, all of the reactions have been accomplished under exactly similar reaction conditions, the optimum reaction conditions. Comparison of the yield of the hydrogenated PAO in Fig. 9 demonstrated that Pd/Hal-Py was recyclable and the decrement of the yield of the reaction after each run was negligible.

To appraise the leaching of Pd nanoparticles upon recycling, the recovered Pd/Hal-Py after fifth run was subjected to ICP analysis. Gratifyingly, ICP analysis approved that the Pd loading of the recycled Pd/Hal-Py (after fourth run) was 1.5 wt% of the initial content.

3.5. Hot filtration test

Two passes are conceivable for the catalysis under Pd/Hal-Py. In one rout, denoted as true heterogeneous, Pd nanoparticles are stabilized on the support in the course of hydrogenation. In the second one, denoted as leaching-redeposition, Pd nanoparticles are leached through the reaction and deposited on the support at the end of the reaction. To verify which pass is followed by the catalyst, hot filtration test was conducted. According to the standard method [65], the hydrogenation reaction of PAO under the optimum conditions was halted after 2 h and then Pd/Hal-Py was separated. The reaction was then followed in the absence of Pd/Hal-Py and the reaction progress was monitored via ^{1}H NMR. The results established that upon removal of the catalyst the reaction did not precede, ruling out the leaching-redeposition pass.

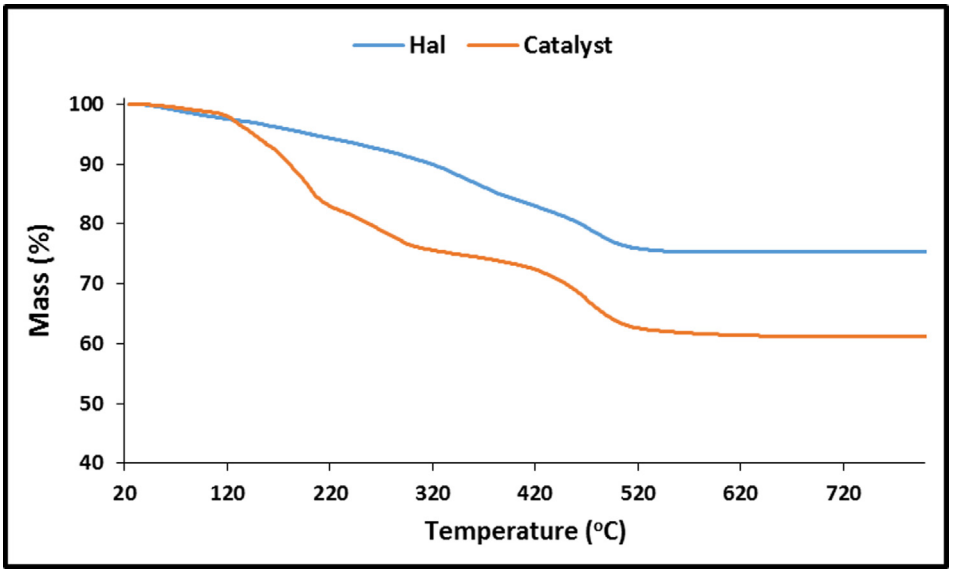

Fig. 8. TG curves of Hal and Pd/Hal-Py.

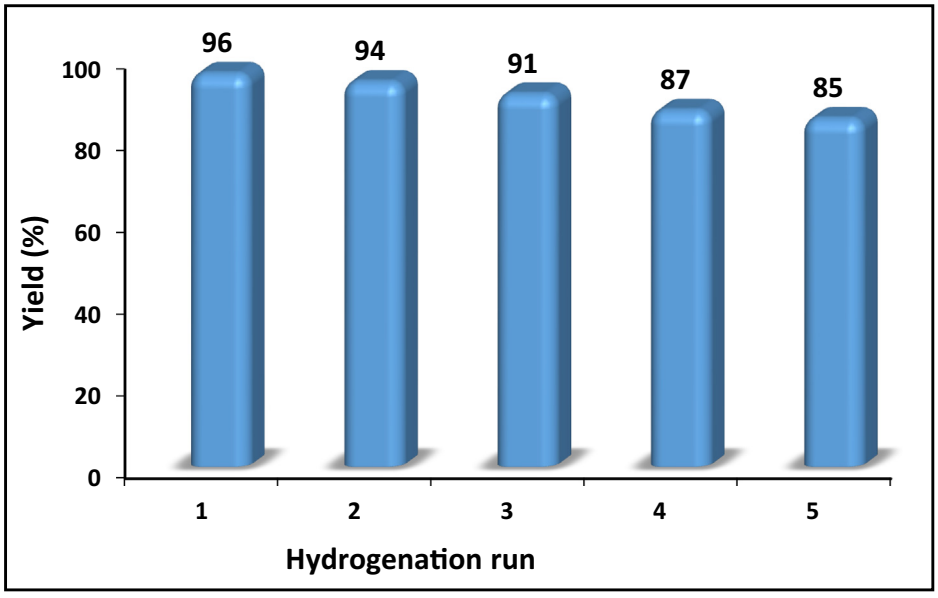

Fig. 9. Comparison of the yield of hydrogenated PAO upon reusing of the catalyst (Reaction conditions: Catalyst: 5 wt%, T = 130 °C and P = 7 bar).

3.6. Structural features of PAO before and after hydrogenation

In the last part of this research, to shed light on the microstructural variation of the as-synthesized PAO by hydrofinishing process, its molecular weight and branching type was surveyed Figs. 10 and 11. The results were gathered in Table 2. In the structural analysis, each CH_3 share was quantified from its related peak intensity to the total peak surface area in ^{13}C NMR spectra. Notably, no considerable change was found in the methyl type quantity before and after hydrofinishing. In both cases, a long chain branching value (sum of $CHCH_2CH_2\mathbf{CH_3}$ and $(CH_2)_nCH_2CH_2\mathbf{CH_3}$, n > 1 moieties) of 42–43 % was obtained for the synthesized PAO. Furthermore, no considerable change in the molecular weight was observed after hydrogenation process. These achieved results acknowledge well the absence of any isomerization, which deteriorate PAO properties, specially its pour point characteristic. This is another confirmation on the ability of designed catalyst in the PAO hydrofinishing process.

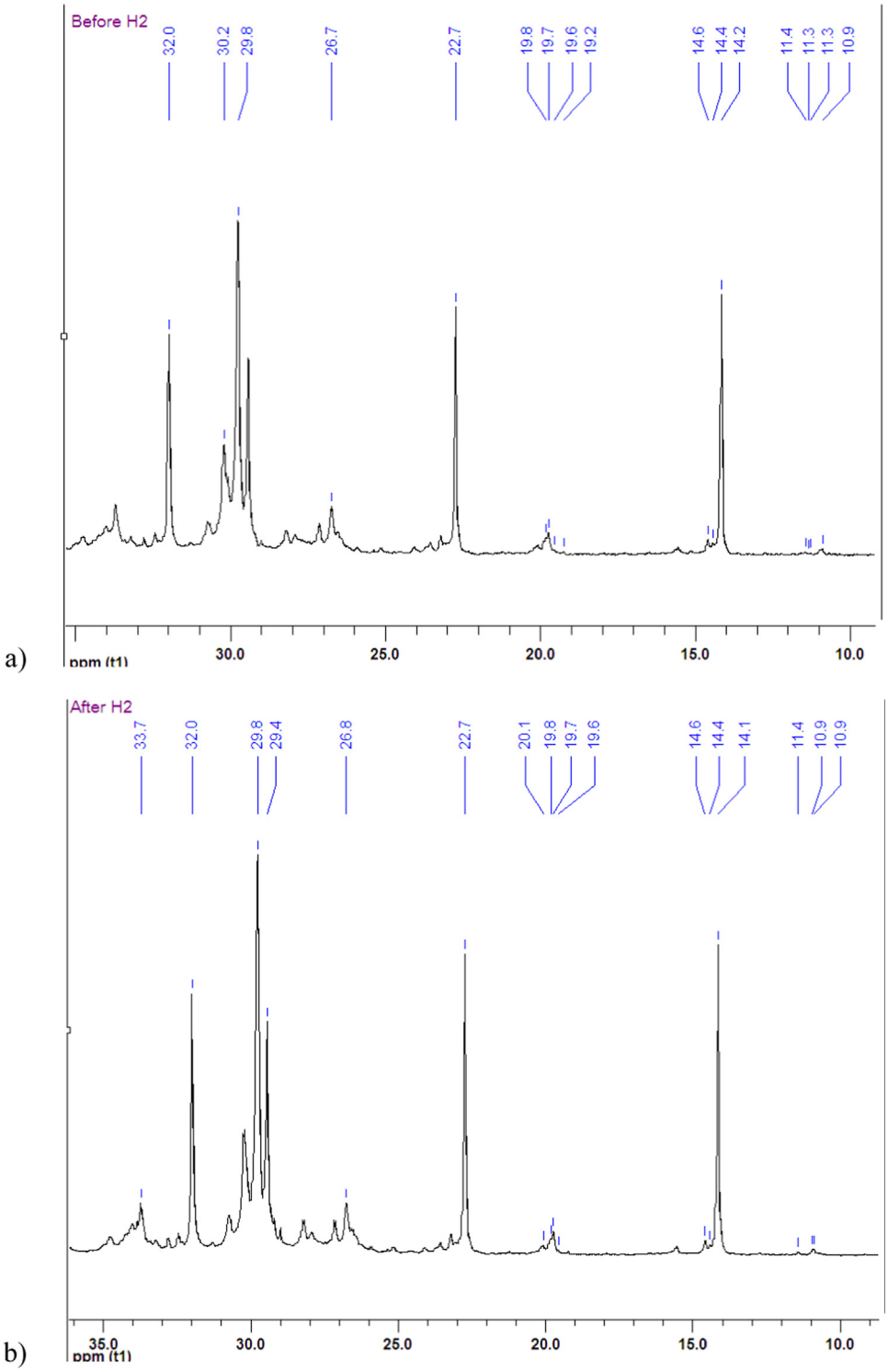

Fig. 10. ^{13}C NMR spectra of the as-synthesized PAO a) before and b) after hydrogenation process.

4. Conclusions

In an attempt to screen the most suitable ligand for the decoration of Hal and designing a suitable catalyst for the hydrogenation of PAO, computationally the insertion of the Pd atom in designed series of catalysts was streamlined using DFT methods, and steric maps. Among the studied catalysts, catalyst **6** revealed the largest binding energy among the designed systems. Here, the flexibility of the proposed ligand unveils that the sterics are not the most important characteristics, but how it can allocate the metal center. Then, the chosen catalyst, **6**, was successfully synthesized and employed in PAO hydrogenation reaction. The values of H_2 pressure, reaction temperature and catalyst dosage were optimized to achieve the highest catalytic performance of 96 % with PAO bromine index of 55 Br/100. No alteration of PAO microstructure, towards molecular weight and branching type, praised the

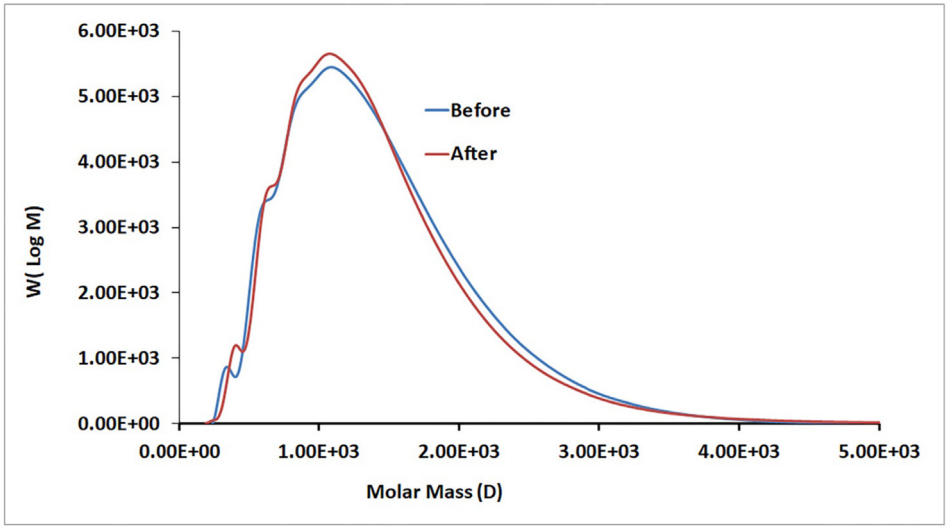

Fig. 11. GPC curves of the synthesized PAO before and after hydrogenation.

Table 2
CH_3 type and molecular weight of the synthesized PAO before and after hydrogenation process.

	Before hydrogenation	After hydrogenation
$CCH_2\mathbf{CH_3}$	1	2
$(CH_3)CHCH_2\mathbf{CH_3}$	1	1
$CHCH_2CH_2\mathbf{CH_3}$	2	3
$CH(CH_3)CH_2CH_2CH_3$	2	2
$(CH_2)_nCH_2CH_2\mathbf{CH_3}$ n > 1	40	40
$CH_2CH\mathbf{(CH_3)}CH$	6	6
$CH_2CH(CH_3)CH_2$	7	4
$CH_3CH(CH_3)CH_2$	41	42
M_n (g/mol)	**921**	**907**
M_w (g/mol)	**1158**	**1140**
PDI	**1.3**	**1.3**

employed strategy (*i.e.* the combination of DFT tool with proper synthetic routes for catalyst synthesis) in designing efficient hydrogenation catalyst for PAO oils.

CRediT authorship contribution statement

Mohammadreza Mehdizadeh: Investigation. **Samahe Sadjadi:** Supervision, Conceptualization. **Albert Poater:** Investigation, Supervision, Conceptualization. **AmirMohammad Mansouri:** . **Naeimeh Bahri-Laleh:** Supervision, Conceptualization.

Declaration of Competing Interest

The authors declare that they have no known competing financial interests or personal relationships that could have appeared to influence the work reported in this paper.

Acknowledgments

The authors appreciate support of Iran Polymer and Petrochemical Institute and University of Girona. A.P. is a Serra Húnter Fellow and ICREA Academia Prize 2019, and thanks the Spanish MINECO for project ref. PGC2018-097722-B-I00.

Appendix A. Supplementary data

Supplementary data to this article can be found online at https://doi.org/10.1016/j.molliq.2022.118675.

References

[1] S. Sadjadi, M. Akbari, B. Léger, E. Monflier, M.M. Heravi, Eggplant-Derived Biochar-Halloysite Nanocomposite as Supports of Pd Nanoparticles for the Catalytic Hydrogenation of Nitroarenes in the Presence of Cyclodextrin, ACS Sustainable Chem. Eng. 7 (7) (2019) 6720–6731.
[2] S. Sadjadi, M. Akbari, E. Monflier, M.M. Heravi, B. Leger, Pd nanoparticles immobilized on halloysite decorated with a cyclodextrin modified melamine-based polymer: a promising heterogeneous catalyst for hydrogenation of nitroarenes, New J. Chem. 42 (2018) 15733–15742.
[3] G. Cavallaro, G. Lazzara, S. Milioto, F. Parisi, Hydrophobically Modified Halloysite Nanotubes as Reverse Micelles for Water-in-Oil Emulsion, Langmuir 31 (27) (2015) 7472–7478.
[4] L. Lisuzzo, G. Cavallaro, S. Milioto, G. Lazzara, Halloysite Nanotubes as Nanoreactors for Heterogeneous Micellar Catalysis, J. Colloid Interface Sci. 608 (2022) 424–434.
[5] G. Lazzara, G. Cavallaro, A. Panchal, R. Fakhrullin, A. Stavitskaya, V. Vinokurov, Y. Lvov, An assembly of organic-inorganic composites using halloysite clay nanotubes, Curr. Opin. Colloid Interface Sci. 35 (2018) 42–50.
[6] V. Akbari, M. Jouyandeh, S.M.R. Paran, M.R. Ganjali, H. Abdollahi, H. Vahabi, Z. Ahmadi, K. Formela, A. Esmaeili, A. Mohaddespour, S. Habibzadeh, M.R. Saeb, Polymers 12 (2020) 930.
[7] G. Cavallaro, G. Lazzara, S. Milioto, F. Parisi, V. Evtugyn, E. Rozhina, R. Fakhrullin, Nanohydrogel Formation within the Halloysite Lumen for Triggered and Sustained Release, ACS Appl. Mater. Interfaces 10 (9) (2018) 8265–8273.
[8] C. Copéret, A. Comas-Vives, M.P. Conley, D. P. Estes, A. Fedorov, V. Mougel H. Nagae, F. Núnez-Zarur, P. A. Zhizhko, Surface Organometallic and Coordination Chemistry toward Single-Site Heterogeneous Catalysts: Strategies, Methods, Structures, and Activities, Chem. Rev. 116 (2016) 323-342.
[9] L. Lisuzzo, G. Cavallaro, S. Milioto, G. Lazzara, Effects of halloysite content on the thermo-mechanical performances of composite bioplastics, Appl. Clay Sci. 185 (2020) 105416.
[10] N. Danyliuk, J. Tomaszewska, T. Tatarchuk, Halloysite nanotubes and halloysite-based composites for environmental and biomedical applications, J. Mol. Liq. 309 (2020) 113077.
[11] P. Yuan, D. Tan, F. Annabi-Bergaya, Properties and applications of halloysite nanotubes: recent research advances and future prospects, Appl. Clay Sci. 112–113 (2015) 75–93.
[12] S. Sadjadi, N. Abedian-Dehaghani, F. Koohestani, M.M. Heravi, Halloysite functionalized with Cu (II) Schiff base complex containing polymer as an efficient catalyst for chemical transformation, Inorg. Chem. Commun. 133 (2021) 108955.
[13] A. Mahajan, P. Gupta, Halloysite nanotubes based heterogeneous solid acid catalysts, New J. Chem. 44 (30) (2020) 12897–12908.
[14] M.J. Baruah, T.J. Bora, R. Dutta, S. Roy, A.K. Guha, K.K. Bania, Fe(III) superoxide radicals in halloysite nanotubes for visible-light-assisted benzyl alcohol oxidation and oxidative CC coupling of 2-naphthol, Mol. Catal. 515 (2021) 111858.
[15] J. Jin, J. Ouyang, H. Yang, Pd Nanoparticles and MOFs Synergistically Hybridized Halloysite Nanotubes for Hydrogen Storage, Nanoscale Res. Lett. 12 (2017) 240.
[16] Z. Zhu, D. Ding, Y. Zhang, Y. Zhang, Preparation of Ni, CoO-supported halloysite nanotube catalyst and its application in the hydrogenation of furfural to furfuryl alcohol, Appl. Clay Sci. 196 (2020) 105761.
[17] S. Sadjadi, M.M. Heravi, M. Malmir, F.G. Kahangi, Ionic-liquid and cuprous sulfite containing halloysite nanoclay: An efficient catalyst for Click reaction as well as N- and O-arylations, Appl. Clay Sci. 162 (2018) 192–203.

[18] S. Sadjadi, M.M. Heravi, M. Raja, Combination of carbon nanotube and cyclodextrin nanosponge chemistry to develop a heterogeneous Pd-based catalyst for ligand and copper free C-C coupling reactions, Carbohydr. Polym. 185 (2018) 48–55.
[19] S. Sadjadi, F. Koohestani, Functionalized chitosan polymerized with cyclodextrin decorated ionic liquid: Metal free and biocompatible catalyst for chemical transformations, Int. J. Biol. Macromol. 147 (2020) 399–407.
[20] F. Karimi, M.A. Zolfigol, M. Yarie, A novel and reusable ionically tagged nanomagnetic catalyst: Application for the preparation of 2-amino-6-(2-oxo-2H-chromen-3-yl)-4-arylnicotinonitriles via vinylogous anomeric based oxidation, Mol. Catal. 463 (2019) 20–29.
[21] S. Sadjadi, M. Akbari, M.M. Heravi, Palladated Nanocomposite of Halloysite–Nitrogen-Doped Porous Carbon Prepared from a Novel Cyano-/Nitrile-Free Task Specific Ionic Liquid: An Efficient Catalyst for Hydrogenation, ACS Omega 4 (2019) 19442–19451.
[22] B.Ö. Öztürk, Ammonium tagged Hoveyda-Grubbs catalysts immobilized on magnetically separable core-shell silica supports for ring-closing metathesis reactions, Micropor. Mesopor. Mat. 267 (2018) 249–256.
[23] R. Teimuri-Mofrad, M. Gholamhosseini-Nazari, E. Payami, S. Esmati, Ferrocene-tagged ionic liquid stabilized on silica-coated magnetic nanoparticles: Efficient catalyst for the synthesis of 2-amino-3-cyano-4H-pyran derivatives under solvent-free conditions, Appl. Organomet. Chem. 32 (2018) e3955.
[24] E. Rafiee, M. Kahrizi, Mechanistic investigation of Heck reaction catalyzed by new catalytic system composed of Fe3O4@OA–Pd and ionic liquids as co-catalyst, J. Mol. Liq. 218 (2016) 625–631.
[25] S. Sadjadi, Magnetic (poly) ionic liquids: A promising platform for green chemistry, J. Mol. Liq. 323 (2021) 114994.
[26] Q. Zhang, B. Wu, R. Song, H. Song, J. Zhang, X. Hu, Preparation, characterization and tribological properties of polyalphaolefin with magnetic reduced graphene oxide/Fe_3O_4, Tribol. Int. 141 (2020) 105952.
[27] A. Hanifpour, N. Bahri-Laleh, M. Nekoomanesh-Haghighi, A. Poater, Coordinative chain transfer polymerization of 1-decene in the presence of a Ti-based diamine bis(phenolate) catalyst: a sustainable approach to produce low viscosity PAOs, Green Chem. 22 (2020) 4617–4626.
[28] A. Hanifpour, N. Bahri-Laleh, M. Nekoomanesh-Haghighi, A. Poater, Group IV diamine bis(phenolate) catalysts for 1-decene oligomerization, Mol. Catal. 493 (2020) 111047.
[29] N. Bahri-Laleh, A. Hanifpour, S.A. Mirmohammadi, A. Poater, M. Nekoomanesh-Haghighi, G. Talarico, L. Cavallo, Computational modeling of heterogeneous Ziegler-Natta catalysts for olefins polymerization, Prog. Polym. Sci. 84 (2018) 89–114.
[30] X. Zhang, M. Fevre, G.O. Jones, R.M. Waymouth, Catalysis as an Enabling Science for Sustainable Polymers, Chem. Rev. 118 (2018) 839–885.
[31] M. Fallah, N. Bahri-Laleh, K. Didehban, A. Poater, Interaction of common cocatalysts in Ziegler-Natta catalyzed olefin polymerization, Appl. Organomet. Chem. 34 (2) (2020) e5333.
[32] S. Gharajedaghi, Z. Mohamadnia, E. Ahmadi, M. Marefat, G. Pareras, S. Simon, A. Poater, N. Bahri-Laleh, Experimental and DFT Study on Titanium-based Half-Sandwich Metallocene Catalysts and their Application for Production of 1-Hexene from Ethylene, Mol Catal. 509 (2021) 111636.
[33] A. Hanifpour, N. Bahri-Laleh, M. Nekoomanesh-Haghighi, A. Poater, 1-Decene Oligomerization by New Complexes Bearing Diamine-Diphenolates Ligands: Effect of Ligand Structure, Appl. Organomet. Chem. 34 (2021) e6227.
[34] A. Hanifpour, M. Hashemzadeh Gargari, M.R. Rostami Darounkola, Z. Kalantari, N. Bahri-Laleh, Kinetic and microstructural studies of Cp_2ZrCl_2 and Cp_2HfCl_2-catalyzed oligomerization of higher α-olefins in mPAO oil base stocks production, Polyolefins J. 8 (2021) 31–40.
[35] S. Gaillard, J.-L. Renaud, Iron-catalyzed hydrogenation, hydride transfer, and hydrosilylation: An alternative to precious-metal complexes?, ChemSusChem (2008) 505–509
[36] S. Sadjadi, F. Koohestani, Palladated composite of Cu-BDC MOF and perlite as an efficient catalyst for hydrogenation of nitroarenes, J. Mol. Struct. 1250 (2022) 131793.
[37] P. Liu, M. Zhao, Silver nanoparticle supported on halloysite nanotubes catalyzed reduction of 4-nitrophenol (4-NP), Appl. Surf. Sci. 255 (7) (2009) 3989–3993.
[38] S. Karimi, N. Bahri-Laleh, G. Pareras, S. Sadjadi, M. Nekoomanesh-Haghighi, A. Poater, Pd on nitrogen rich polymer–halloysite nanocomposite as an environmentally benign and sustainable catalyst for hydrogenation of polyalfaolefin based lubricants, J. Ind. Eng. Chem. 97 (2021) 441–451.
[39] M.J. Frisch, G.W. Trucks, H.B. Schlegel, G.E. Scuseria, M.A. Robb, J.R. Cheeseman, G. Scalmani, V. Barone, B. Mennucci, G.A. Petersson, H. Nakatsuji, M. Caricato, X. Li, H.P. Hratchian, A.F. Izmaylov, J. Bloino, G. Zheng, J.L. Sonnenberg, M. Hada, M. Ehara, K. Toyota, R. Fukuda, J. Hasegawa, M. Ishida, T. Nakajima, Y. Honda, O. Kitao, H. Nakai, T. Vreven, J.A. Montgomery, J.E. Peralta, F. Ogliaro, M. Bearpark, J.J. Heyd, E. Brothers, K.N. Kudin, V.N. Staroverov, R. Kobayashi, J. Normand, K. Raghavachari, A. Rendell, J.C. Burant, S.S. Iyengar, J. Tomasi, M. Cossi, N. Rega, J.M. Millam, M. Klene, J.E. Knox, J.B. Cross, V. Bakken, C. Adamo, J. Jaramillo, R. Gomperts, R.E. Stratmann, O. Yazyev, A.J. Austin, R. Cammi, C. Pomelli, J.W. Ochterski, R.L. Martin, K. Morokuma, V.G. Zakrzewski, G.A. Voth, P. Salvador, J.J. Dannenberg, S. Dapprich, A.D. Daniels, Ö. Farkas, J.B. Foresman, J.V. Ortiz, J. Cioslowski, D.J. Fox, Gaussian 16, Gaussian Inc., Wallingford CT, 2016.
[40] A.D. Becke, Density-functional thermochemistry. III. The role of exact exchange, J. Chem. Phys. 98 (7) (1993) 5648–5652.
[41] C. Lee, W. Yang, R.G. Parr, Development of the Colle-Salvetti correlation-energy formula into a functional of the electron density, Phys. Rev. B 37 (2) (1988) 785–789.
[42] P.J. Stephens, F.J. Devlin, C.F. Chabalowski, M.J. Frisch, Ab Initio Calculation of Vibrational Absorption and Circular Dichroism Spectra Using Density Functional Force Fields, J. Phys. Chem. 98 (45) (1994) 11623–11627.
[43] F. Weigend, R. Ahlrichs, Balanced basis sets of split valence, triple zeta valence and quadruple zeta valence quality for H to Rn: Design and assessment of accuracy, Phys. Chem. Chem. Phys. 7 (18) (2005) 3297.
[44] F. Weigend, Accurate Coulomb-fitting basis sets for H to Rn, Phys. Chem. Chem. Phys. 8 (9) (2006) 1057.
[45] U. Häussermann, M. Dolg, H. Stoll, H. Preuss, P. Schwerdtfeger, R. Pitzer, Accuracy of energy-adjusted quasirelativistic ab initio pseudopotentials: all-electron and pseudopotential benchmark calculations for Hg, HgH and their cations, Mol. Phys. 78 (1993) 1211–1224.
[46] W. Küchle, M. Dolg, H. Stoll, H. Preuss, Energy-adjusted pseudopotentials for the actinides. Parameter sets and test calculations for thorium and thorium monoxide, J. Chem. Phys. 100 (10) (1994) 7535–7542.
[47] T. Leininger, A. Nicklass, H. Stoll, M. Dolg, P. Schwerdtfeger, The accuracy of the pseudopotential approximation. II. A comparison of various core sizes for indium pseudopotentials in calculations for spectroscopic constants of InH, InF, and InCl, J. Chem. Phys. 105 (3) (1996) 1052–1059.
[48] S. Sadjadi, F. Koohestani, G. Pareras, M. Nekoomanesh-Haghighi, N. Bahri-Laleh, A. Poater, Combined experimental and computational study on the role of ionic liquid containing ligand in the catalytic performance of halloysite-based hydrogenation catalyst, J. Mol. Liq. 331 (2021) 115740.
[49] A.V. Marenich, C.J. Cramer, D.G. Truhlar, Universal solvation model based on solute electron density and on a continuum model of the solvent defined by the bulk dielectric constant and atomic surface tensions, J. Phys. Chem. B 113 (18) (2009) 6378–6396.
[50] S. Grimme, J. Antony, S. Ehrlich, H. Krieg, A consistent and accurate ab initio parametrization of density functional dispersion correction (DFT-D) for the 94 elements H-Pu, J. Chem. Phys. 132 (2010) 154104.
[51] L. Falivene, V. Barone, G. Talarico, Unraveling the role of entropy in tuning unimolecular vs. bimolecular reaction rates: the case of olefin polymerization catalyzed by transition metals, Mol. Catal. 452 (2018) 138–144.
[52] L. Falivene, R. Credendino, A. Poater, A. Petta, L. Serra, R. Oliva, V. Scarano, L. Cavallo, SambVca 2, A Web Tool for Analyzing Catalytic Pockets with Topographic Steric Maps, Organometallics 35 (13) (2016) 2286–2293.
[53] L. Falivene, Z. Cao, A. Petta, L. Serra, A. Poater, R. Oliva, V. Scarano, L. Cavallo, Towards the online computer-aided design of catalytic pockets, Nat. Chem. 11 (10) (2019) 872–879.
[54] M. Tabrizi, S. Sadjadi, G. Pareras, M. Nekoomanesh-Haghighi, N. Bahri-Laleh, A. Poater, Efficient hydro-finishing of polyalfaolefin based lubricants under mild reaction condition using Pd on ligands decorated halloysite, J. Colloid Interface Sci. 581 (2021) 939–953.
[55] S. Dehghani, S. Sadjadi, N. Bahri-Laleh, M. Nekoomanesh-Haghighi, A. Poater, Study of the effect of the ligand structure on the catalytic activity of Pd@ ligand decorated halloysite: Combination of experimental and computational studies, Appl. Organomet. Chem. 33 (2019) e4891.
[56] N. Bahri-Laleh, S. Sadjadi, A. Poater, Pd immobilized on dendrimer decorated halloysite clay: Computational and experimental study on the effect of dendrimer generation, Pd valance and incorporation of terminal functionality on the catalytic activity, J. Colloid Interface Sci. 531 (2018) 421–432.
[57] S. Kaur, V. Kumar, M. Chawla, L. Cavallo, A. Poater, N. Upadhyay, Pesticides Curbing Soil Fertility: Effect of Complexation of Free Metal Ions, Front. Chem. 5 (2017) 43.
[58] M. Tomasini, J. Duran, S. Simon, L.M. Azofra, A. Poater, Towards Mild Conditions by Predictive Catalysis via Sterics in the Ru-Catalyzed Hydrogenation of Thioesters, Mol. Catal. 510 (2021) 111692.
[59] D. Peral, F. Gómez-Villarraga, X. Sala, J. Pons, J. Carles Bayón, J. Ros, M. Guerrero, L. Vendier, J.P. Lecante, K.P. García-Antón, Catal, Sci. Technol. 3 (2013) 475–489.
[60] L. Chen, H. Chen, R. Luque, Y. Li, Metal−organic framework encapsulated Pd nanoparticles: Towards advanced heterogeneous catalysts, Chem. Sci. 3708–3714 (2014).
[61] S. Sadjadi, Halloysite-based hybrids/composites in catalysis, Appl. Clay Sci. 189 (2020) 105537.
[62] H. Zhu, MingLiang Du, MeiLing Zou, CongSheng Xu, YaQin Fu, Green synthesis of Au nanoparticles immobilized on halloysite nanotubes for surface-enhanced Raman scattering substrates, Dalton Trans. 41 (34) (2012) 10465.
[63] P. Yuan, P.D. Southon, Z. Liu, M.E.R. Green, J.M. Hook, S.J. Antill, C.J. Kepert, Functionalization of Halloysite Clay Nanotubes by Grafting with γ-Aminopropyltriethoxysilane, J. Phys. Chem. C 112 (40) (2008) 15742–15751.
[64] S. Mallik, S.S. Dash, K.M. Parida, B.K. Mohapatra, Synthesis, characterization, and catalytic activity of phosphomolybdic acid supported on hydrous zirconia, J. Colloid Interface Sci. 300 (1) (2006) 237–243.
[65] T. Baran, N. Yılmaz Baran, A. Menteş, Highly active and recyclable heterogeneous palladium catalyst derived from guar gum for fabrication of biaryl compounds, Int. J. Biol. Macromol. 132 (2019) 1147–1154.